Bioactive Materials 5 (2020) 542–552

Contents lists available at ScienceDirect

Bioactive Materials

journal homepage: http://www.keaipublishing.com/biomat

Near-infrared responsive 5-fluorouracil and indocyanine green loaded MPEG-PCL nanoparticle integrated with dissolvable microneedle for skin cancer therapy

Ying Hao[a], YuWen Chen[a], XinLong He[a], Fan Yang[a], RuXia Han[a], ChengLi Yang[a], Wei Li[b], ZhiYong Qian[a,*]

[a] State Key Laboratory of Biotherapy and Cancer Center, West China Hospital, Sichuan University, and Collaborative Innovation Center of Biotherapy, Chengdu, 610041, PR China

[b] Department of Dermatovenereology, West China Hospital, Sichuan University, Chengdu, 610041, PR China

ARTICLE INFO

Keywords:
5-Fluorouracil (5-Fu)
Indocyanine green (ICG)
Monomethoxy-poly (ethylene glycol)-polycaprolactone (MPEG-PCL)
Hyaluronic acid dissolvable microneedle (HA MN)
Skin cancer

ABSTRACT

The prevalence of skin cancer is rising along with the rapid population aging in recent years. Traditional therapies, such as surgical treatment, radiotherapy, chemotherapy, photodynamic therapy, and immunotherapy, may accompany serious side effects, limiting their clinical benefits. According to the biological characteristics of skin cancer, we have already established two kinds of synergetic systems of photothermal therapy (microneedle) and chemotherapy, containing gold nanorods (GNR). Although the microneedle system exhibited great potential for skin cancer treatment, the system could be still improved further. So, we designed a near-infrared light-responsive 5-fluorouracil (5-Fu) and indocyanine green (ICG) loaded monomethoxy-poly (ethylene glycol)-polycaprolactone (MPEG-PCL) nanoparticle (5-Fu-ICG-MPEG-PCL), and then 5-Fu-ICG-MPEG-PCL was integrated with a hyaluronic acid dissolvable microneedle system (HA MN) to get 5-Fu-ICG-MPEG-PCL loaded HA MN for treating skin cancers, including human epidermoid cancer and melanoma. In this system, hyaluronic acid, the microneedle carrier, possesses good skin penetration ability and is approved by FDA as a pharmaceutical adjuvant; 5-Fu is recommended by FDA for skin cancer treatment; ICG, a photothermal agent, possesses a strong photothermal ability and is approved by FDA for its use in the human body. We hypothesized that 5-Fu-ICG-MPEG-PCL could be delivered by the dissolvable microneedle through the skin, and the release behavior of the drug in the nanoparticle could be controlled by near-infrared light for achieving a single-dose cure of skin cancer, improving the cure rate of skin cancer and providing a new idea and possibility for the clinical treatment of skin cancer.

1. Introduction

Skin cancer is a malignant tumor originating from cutaneous keratinocytes. Skin squamous cell carcinoma, basal cell carcinoma, and melanoma are the most common forms of clinical skin cancer [1]. The prevalence of skin cancer is gradually increasing along with China's population aging [2,3]. Surgical treatment, radiotherapy, chemotherapy, photodynamic therapy, and immunotherapy are commonly used for skin cancer treatment. But these traditional therapies exhibited some obvious limitations [4–7]. For overcoming these challenges, we should explore newer therapies for skin cancer treatment.

Microneedles or microscale needle tip structure are fabricated by the micro-nano processing technology. They can penetrate the cuticle of the skin and enter the dermis through the acanthocyte and basal cell layers [8,9]. Microneedles are widely used in recent years for improving the transdermal absorption capacity of a drug [10,11]. Moreover, the microneedle system can transport drugs, proteins, genes, RNA, vaccines, and other biological macromolecules, and they are highly efficient, convenient and harmless [12,13]. Compared to the oral or parenteral drug delivery system, the transdermal microneedles can penetrate the cuticle of the skin to directly deliver the drug, thus bypassing the first-pass effect of the liver, avoiding the gastrointestinal degradation, improving the bioavailability and reducing the side effects of the drugs [14,15]. Combined with the biological characteristics of skin cancer, the microneedle-based drug delivery system is a better drug carrier for skin cancer treatment. Recently, the microneedle-based

Peer review under responsibility of KeAi Communications Co., Ltd.
* Corresponding author.
E-mail address: anderson-qian@163.com (Z. Qian).

https://doi.org/10.1016/j.bioactmat.2020.04.002
Received 15 March 2020; Received in revised form 5 April 2020; Accepted 5 April 2020

transdermal drug delivery system has provided a broad application prospect for skin cancer treatment [16–18].

In a previous study, we have already developed two kinds of synergetic systems of photothermal therapy (microneedle) and chemotherapy, containing gold nanorods (GNR). Firstly, we used poly (L-lactide) microneedle (PLLA MN) to absorb PEGylated gold nanorod (GNR-PEG) and obtained GNR-PEG loaded PLLA MN (GNR-PEG@MNs) with good heating efficacy. Then, we utilized the GNR-PEG@MNs and docetaxel loaded MPEG-PDLLA micelles to treat epidermoid cancer. The combination of GNR-PEG@MNs and MPEG-PDLLA-DTX micelles at a low dose (5 mg/kg) efficiently prevented the tumor growth and cured all mice without recurrence [19]. Although this system demonstrated a good therapeutic effect, it required multiple intravenous administration. Therefore, we constructed a PEGylated gold nanorod (GNR-PEG) and doxorubicin (DOX) loaded dissolvable hyaluronic acid (HA) microneedle (GNR-PEG&DOX@HA MN) to eliminate the tumor. This microneedle system exhibited strong photothermal effect and heat-transfer efficacy, which could burn the tumor tissue and effectively inhibit epidermal cancer. *In vivo* anti-tumor study revealed that the GNR-PEG&DOX@HA MN could potentially treat epidermal cancer [20]. However, the microneedle system exhibited uncontrollable drug release as its major disadvantage.

Herein, we designed a near-infrared light-responsive 5-fluorouracil (5-Fu) and indocyanine green (ICG) loaded monomethoxy-poly (ethylene glycol)-polycaprolactone (MPEG-PCL) nanoparticle (5-Fu-ICG-MPEG-PCL), and then the 5-Fu-ICG-MPEG-PCL was integrated with a hyaluronic acid dissolvable microneedle system (HA MN) to obtain 5-Fu-ICG-MPEG-PCL loaded HA MN (5-Fu-ICG-MPEG-PCL@HA MN) for treating skin cancers, including human epidermoid cancer and melanoma (Fig. 1). In this system, we selected MPEG-PCL with good biocompatibility and biodegradability to load 5-Fu and ICG by double emulsion method. The chemotherapy drug, 5-Fu, is recommended for treating epidermal cancer in clinic [21,22]. The photothermal agent, ICG, exhibited strong photothermal ability and approved by the U.S. Food and Drug Administration (FDA) for use in humans [23,24]. Moreover, we combined the 5-Fu-ICG-MPEG-PCL with the microneedle system by the template method. The microneedle material hyaluronic acid (HA) displayed good skin penetration ability and has been approved by the FDA as pharmaceutical excipients [25,26]. The 5-Fu-ICG-MPEG-PCL@HA MN having a length of 600 μm displayed high drug loading ability. When the 5-Fu-ICG-MPEG-PCL@HA MN was inserted into the tumor tissue with an 808 nm NIR laser, the ICG in the nanoparticles could transform the light energy into heat energy, which burned the tumor tissue and killed the tumor cells. Also, ICG could control the release behavior of 5-Fu in the nanoparticles to achieve optimum chemotherapy and photothermal therapy for skin cancer treatment. This microneedle system could achieve a single-dose cure for skin cancer and provide a new idea and possibility for clinical treatment of skin cancer.

2. Materials and methods

2.1. Materials

Indocyanine green (ICG), monomethoxy-poly (ethylene glycol) (MPEG, Mn = 5000), ε-caprolactone (ε-CL), stannous octoate (Sn $(Oct)_2$), trypan blue and polyvinyl alcohol (PVA) were obtained from Sigma Aldrich Company, and 5-fluorouracil (5-Fu) was purchased from Meilun biology technology Co., Ltd (Dalian, China). Sodium hyaluronic acid (Mn = 1.44×10^3 kDa) was purchased from Freda Biochem Co. Ltd (Shandong China). All the chemicals were of analytic grade and used as received.

2.2. Synthesis and characterization of MPEG-PCL

The diblock polymer monomethoxy-poly (ethylene glycol)-polycaprolactone (MPEG-PCL, 5000–30000) was synthesized via ring-opening polymerization of MPEG and ε-CL, following a previously reported method [27]. Then, the diblock polymer MPEG-PCL was characterized by ^{1}HNMR spectra (Varian 400 spectrometer, Varian, USA), FTIR (NICOLET 200SXV, Nicolet, USA), and GPC (Agilent 110 HPLC, USA).

2.3. Preparation and characterization of 5-Fu-ICG-MPEG-PCL nanoparticle

We used the double emulsion method to prepare ICG and 5-Fu loaded MPEG-PCL nanoparticles (5-Fu-ICG-MPEG-PCL) as described before [28] (Fig. 2A). Briefly, 0.5 mL of ICG and 5-Fu dissolved in water and added dropwise into 4 mL of dichloromethane, containing 10 mg of MPEG-PCL, and ultrasonicated via a probe-type ultrasonic device. Then, the primary emulsion was added dropwise into 10 mL of 0.1% PVA phosphate-buffered saline and ultrasonicated again, the dichloromethane was removed by rotary evaporation under vacuum. The unloaded 5-Fu and ICG were centrifuged to get ICG and 5-Fu loaded nanoparticles. The control group (MPEG-PCL), ICG loaded MPEG-PCL nanoparticle (ICG-MPEG-PCL) and 5-Fu loaded MPEG-PCL nanoparticle (5-Fu-MPEG-PCL) were prepared following the same method. Next, we used dynamic light scattering (DLS), transmission electron microscopy (TEM) and ultraviolet spectrophotometer (UV) to characterize the nanoparticles.

2.4. Light controlled release behavior of 5-Fu-ICG-MPEG-PCL

The light-controlled release behavior of 5-Fu-ICG-MPEG-PCL was evaluated by the modified dialysis method [29]. In detail, 0.8 mL of 5-Fu, 5-Fu-MPEG-PCL, and 5-Fu-ICG-MPEG-PCL (1 mg/mL) were placed into a dialysis bag with a molecular mass cut off 3500. The dialysis bags were incubated in 10 mL of PBS (pH = 7.4) with gentle shaking at 100 rpm in the gas bath at 37 °C, and then used pre-warmed fresh PBS to replace the media at specific intervals. For the irradiation group, the 5-Fu-ICG-MPEG-PCL was irradiated under 808 nm NIR laser at 1.5 W/cm^2 for 5 min at the predetermined time points, then the medium was collected and replaced with fresh medium. The released drug, 5-Fu, was quantified by HPLC.

2.5. In vitro cytotoxicity assay of 5-Fu-ICG-MPEG-PCL

In vitro cytotoxicity of 5-Fu-ICG-MPEG-PCL was evaluated using human epidermoid cancer cell line A431 and human melanoma cell line A375 via MTT assay. Briefly, the cells were seeded at a density of 4×10^3 cells per well in 96-well plates and incubated for 24 h. Then 100 μL of different nanoparticles with different concentrations were added to each well. After incubating for 24 h (48 h), 20 μL of MTT (5 mg/mL) was added. After 4 h, the medium in 96-well plates was replaced by 150 μL of DMSO, and a microplate reader (Thermo MK3, USA) was used to measure the absorbance of individual wells at 570 nm. Moreover, mouse fibroblast cell line 3T3 were used to study the cytotoxicity of the MPEG-PCL nanoparticle.

2.6. The cellular uptake efficiency of 5-Fu-ICG-MPEG-PCL

Human epidermoid cancer cell line A431 and human melanoma cell line A375 were used to study the cellular uptake efficiency of 5-Fu-ICG-MPEG-PCL, and the photothermal agent, ICG, was used for imaging. In details, a density of 5×10^5 A431 or A375 cells were seeded onto 6-well plates and incubated for 24 h. Then, the medium was replaced by 2 mL of 5-Fu-ICG-MPEG-PCL (25 ng/mL) and incubated for 1 h, 2 h, and 4 h. After removing the supernatant, 70% EtOH was used to fix the cells for 15 min and then DAPI was used to stain the cell nucleus for 10 min. At last, PBS (pH = 7.4) was used to wash the cells 3 times, and then the cells were sealed with glycerin. The cellular uptake efficiency was studied qualitatively under a fluorescence microscope (OLYMPUS,

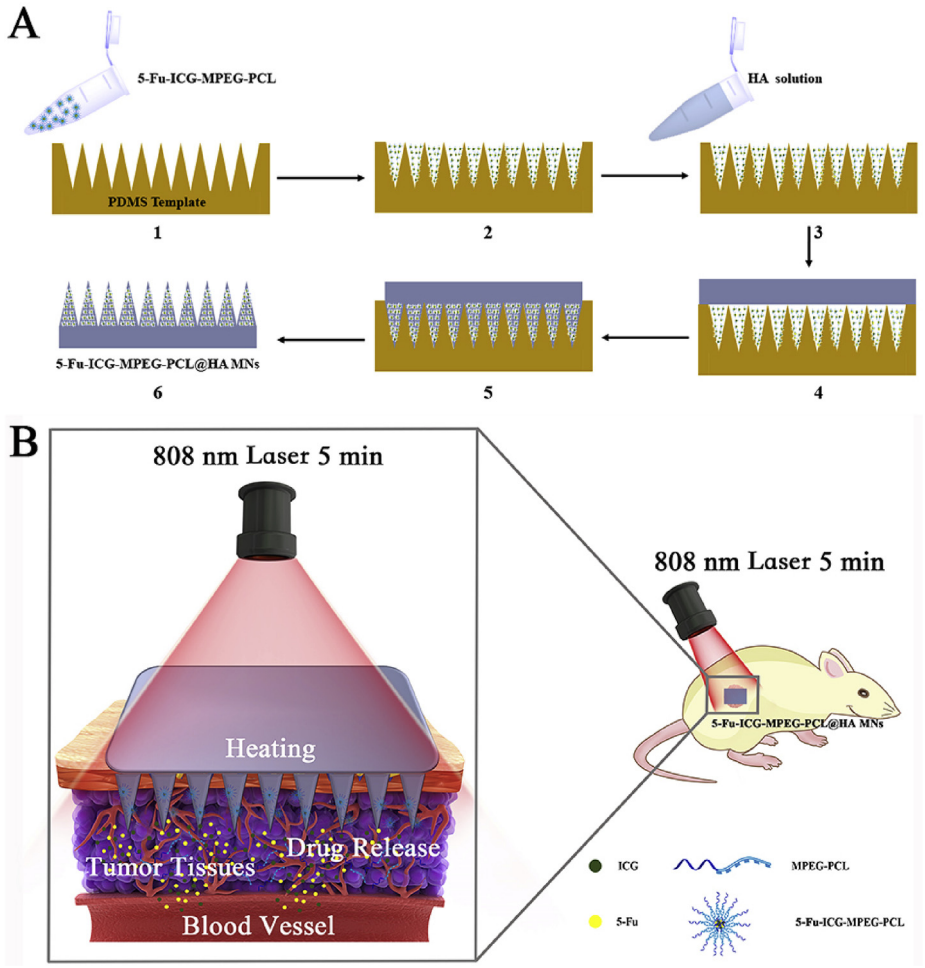

Fig. 1. (A) The preparation process of near-infrared responsive 5-Fu-ICG-MPEG-PCL@HA MN, (B) The schematic illustration of the skin cancer treatment by 5-Fu-ICG-MPEG-PCL@HA MN under 808 nm laser within 5 min (1. The 5-Fu-ICG-MPEG-PCL was poured into the PDMS microneedle master structure; 2. centrifuged, and removed excess 5-Fu-ICG-MPEG-PCL; 3. the HA solution was poured on the PDMS template and 4. centrifuged; 5. the filled mold was dried in an oven at 45 °C overnight; 6. the as-prepared 5-Fu-ICG-MPEG-PCL@HA MN was taken from the PDMS mold gently.)

Germany).

2.7. In vitro photothermal effect of 5-Fu-ICG-MPEG-PCL

We investigated the photothermal effect [30] of 5-Fu-ICG-MPEG-PCL via human epidermoid cancer cell line A431 and human melanoma cell line A375. Firstly, the cells were seeded onto 12-well plates and incubated for 24 h; MPEG-PCL, 5-Fu, 5-Fu-MPEG-PCL, ICG, ICG-MPEG-PCL, and 5-Fu-ICG-MPEG-PCL were added successively. After incubating for 6 h, we used fresh DMEM to replace the medium of each sample. The irradiation groups were treated with an 808 nm NIR laser at 1.5 W/cm^2 for 5 min. Then, the cells were washed with PBS and stained with calcein AM and PI. Finally, we washed the cells with PBS and glycerin and then observed under a fluorescence microscope.

2.8. Preparation and characterization of microneedle

We prepared 5-Fu-ICG-MPEG-PCL loaded microneedle (5-Fu-ICG-MPEG-PCL@HA MN) as described before [31] (Fig. 1A). Briefly, 5-Fu-ICG-MPEG-PCL was poured into the PDMS microneedle master structure and centrifuged. Then, we removed the excess 5-Fu-ICG-MPEG-PCL and poured the HA solution on the PDMS template. Finally, the filled mold was dried in an oven at 45 °C overnight, and taken out from the PDMS mold gently to get 5-Fu-ICG-MPEG-PCL@HA MN. Next, we characterized the morphology and skin insert ability of 5-Fu-ICG-MPEG-PCL@HA MN by scanning electron microscopy (SEM) and trypan blue staining method.

2.9. In vitro near-infrared thermal imaging and heating transfer efficacy

Herein, we investigated the *in vitro* photothermal effect and heat-transfer efficacy of HA MN, 5-Fu-MPEG-PCL@HA MN, ICG-MPEG-PCL@HA MN, 5-Fu-ICG-MPEG-PCL@HA MN by NIR thermal camera (Fluke Ti32, USA), following a previous study [20].

2.10. In vivo near-infrared thermal imaging

Herein, we performed the *in vivo* NIR thermal imaging study via A431 tumor-bearing balb/cA-nu mice and A375 tumor-bearing balb/cA-nu mice. When the tumor volumes of A431 tumor-bearing balb/cA-nu mice and A375 tumor-bearing balb/cA-nu mice were about 200 mm^3, the mice were divided into 8 groups listed below (3 mice per group): (1) the control group, (2) HA MN group, (3) 5-Fu-MPEG-PCL (intratumor) group, (4) ICG-MPEG-PCL (intratumor) group, (5) 5-Fu-ICG-MPEG-PCL (intratumor) group, (6) 5-Fu-MPEG-PCL@HA MN group, (7) ICG-MPEG-PCL@HA MN group, and (8) 5-Fu-ICG-MPEG-PCL@HA MN group. The mice of (3) (4) (5) groups were injected with the above drug intratumorally and irradiated by 808 nm laser (1.5 W/cm^2) for 5 min. The mice of (2) (6) (7) (8) groups were inserted with the above microneedles into the tumor sites from the skin surface and

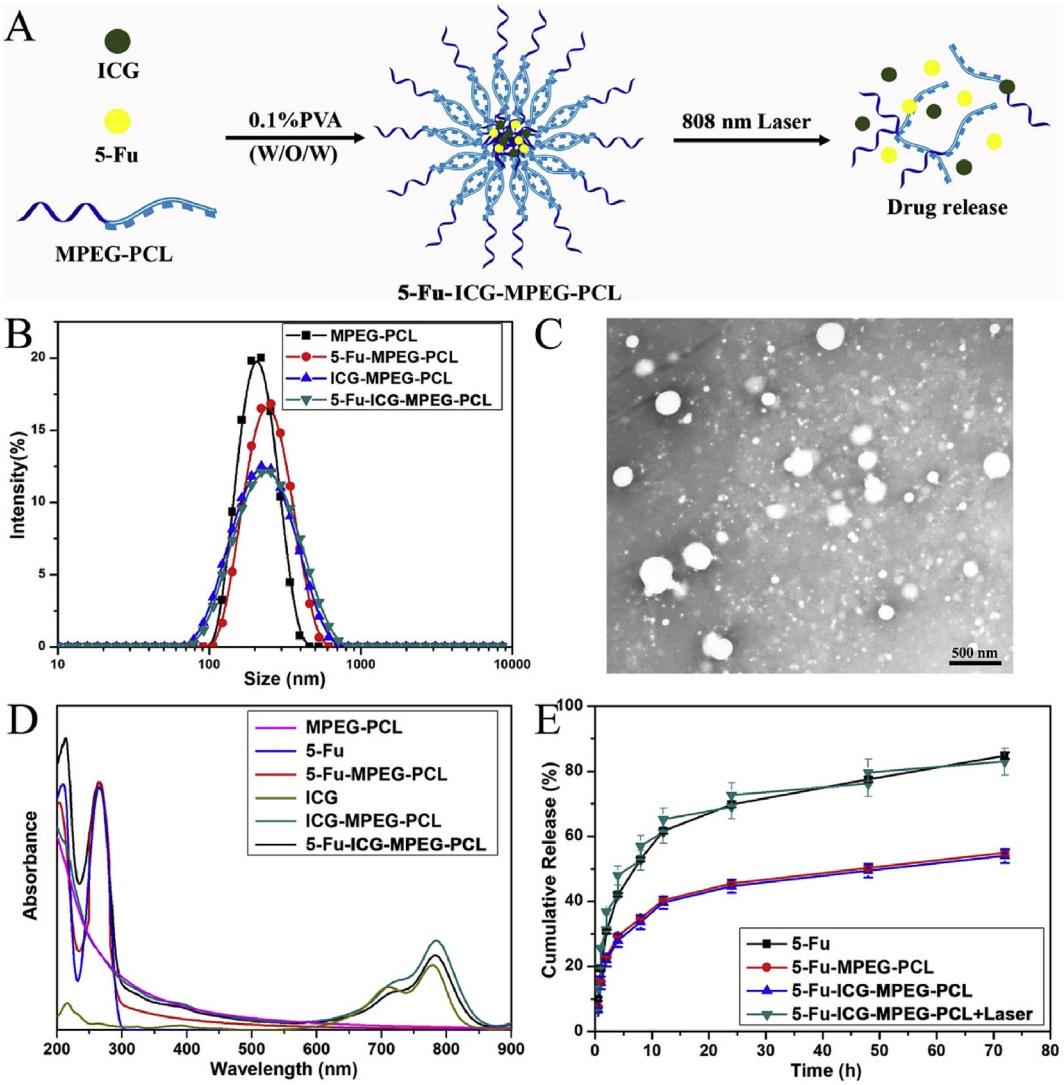

Fig. 2. (A) The schematic illustration of the preparation of 5-Fu-ICG-MPEG-PCL, (B) the particle size of the nanoparticles, (C) the TEM image of 5-Fu-ICG-MPEG-PCL, (D) the ultraviolet absorption and (E) drug release behavior of the nanoparticles.

irradiated by 808 nm laser (1.5 W/cm^2) for 5 min; the control group tumor was irradiated by 808 nm laser (1.5 W/cm^2) for 5 min. Then the mice were imaged at an appropriate time by NIR thermal camera (Fluke Ti32, USA).

2.11. *In vivo* antitumor efficacy

The *in vivo* antitumor efficacy of 5-Fu-ICG-MPEG-PCL@HA MN was carried using A431 tumor-bearing balb/cA-nu mice and A375 tumor-bearing balb/cA-nu mice. In short, the right flank of the mice was injected with 100 μL of 5 × 10^6 A431 cells (A375 cells) subcutaneously. When the volume of subcutaneous tumors was palpable, the mice were divided into 8 groups randomly (5 mice per group): (1) the control group (without treatment); (2) HA MN group, in which HA MN was inserted into the tumor sites transcutaneously; (3) the 5-Fu-MPEG-PCL group, in which 5-Fu-MPEG-PCL was injected intratumorly; (4) ICG-MPEG-PCL + laser group, in which ICG-MPEG-PCL was injected intratumorly and irradiated under 1.5 W/cm^2 NIR laser for 5 min; (5)5-Fu-ICG-MPEG-PCL + laser group, in which 5-Fu-ICG-MPEG-PCL was injected intratumorly and irradiated under 1.5 W/cm^2 NIR laser for 5 min; (6) 5-Fu-MPEG-PCL@HA MN group, in which 5-Fu-MPEG-PCL@HA MN was inserted into the tumor sites transcutaneous; (7) ICG-MPEG-PCL@HA MN + laser group, in which ICG-MPEG-PCL@HA MN was inserted into the tumor sites from the skin surface and irradiated under 1.5 W/cm^2 NIR laser for 5 min; (8) 5-Fu-ICG-MPEG-PCL@HA MN + laser group, in which 5-Fu-ICG-MPEG-PCL@HA MN was penetrated into the tumor sites and irradiated under 1.5 W/cm^2 NIR laser for 5 min. The mice were treated once with the above-mentioned drugs, and the tumor size and body weight were measured every two days. At last, the mice in each group were killed, and the major tissues were collected for hematoxylin and eosin (H&E) staining [32].

2.12. *Histopathological and proliferation study of the tumor cells*

We further performed the histopathological and immune histochemical studies of all groups (3 mice per group) via H&E staining, tunel staining, and Ki67 staining [33].

2.13. *Statistical analysis*

Statistical analysis was performed using Prism 6.0 and Origin 8.0 software. All data in this study were expressed as the mean value ± SD. Student's t-test or one-way analysis of variance (ANOVA) was used for statistical analysis. The difference between the means was considered statistically significant at $P < 0.05$.

3. Results and discussion

3.1. Preparation and characterization of 5-Fu-ICG-MPEG-PCL nanoparticle

We prepared the diblock polymer monomethoxy-poly (ethylene glycol)-polycaprolactone (MPEG-PCL, 5000–30000) via ring-opening polymerization [27] successfully (Fig. S1). Then, we obtained the 5-Fu-ICG-MPEG-PCL nanoparticle using double emulsion method [28]. According to Fig. 2B, the particle sizes of MPEG-PCL, 5-Fu-MPEG-PCL, ICG-MPEG-PCL, and 5-Fu-ICG-MPEG-PCL were 201.6 ± 1.27 nm, 228.8 ± 1.30 nm, 208.1 ± 0.80 nm, and 217.6 ± 0.65 nm, respectively. Moreover, the TEM image (Fig. 2C) demonstrated that the dispersion of 5-Fu-ICG-MPEG-PCL was good, and the particle size was consistent with that measured by dynamic light scattering. In addition, we also characterized the nanoparticle via ultraviolet spectrophotometer (UV), and the UV spectrum of 5-Fu-ICG-MPEG-PCL showed the characteristic absorption peaks of 5-Fu and ICG (Fig. 2D), which implied the successful preparation of 5-Fu-ICG-MPEG-PCL. Additionally, we also investigated the release behavior of 5-Fu-ICG-MPEG-PCL under the NIR light. According to Fig. 2E, the free drug 5-Fu exhibited the fastest releases of 5-Fu-MPEG-PCL and 5-Fu-ICG-MPEG-PCL group, and the release behavior of 5-Fu-ICG-MPEG-PCL + laser could be accelerated by NIR laser, further demonstrated that the 5-Fu-ICG-MPEG-PCL nanoparticle could realize NIR-responsive drug release.

3.2. In vitro cytotoxicity assay of 5-Fu-ICG-MPEG-PCL

We studied the cytotoxicities of 5-Fu-ICG-MPEG-PCL and MPEG-PCL via MTT methods. According to Fig. 3A, the 3T3 cell viability of MPEG-PCL was 43% and 31% higher after 24 h and 48 h incubation, respectively, even when the nanoparticle concentration reached 2 mg/mL, demonstrating that MPEG-PCL exhibited low cellular toxicity, and was a safe drug carrier. Additionally, we also performed the cell viability assay of ICG, ICG-MPEG-PCL, 5-Fu, 5-Fu-MPEG-PCL, and 5-Fu-ICG-MPEG-PCL on A431 and A375 cells. In Fig. 3B-E, the cell viability assay of 5-Fu, 5-Fu-MPEG-PCL, 5-Fu-ICG-MPEG-PCL exhibited dose-dependent function, and 5-Fu-MPEG-PCL, 5-Fu-ICG-MPEG-PCL displayed the cell inhibition ability almost similar to 5-Fu. For both A431 and A375 cells, 48 h of incubation showed a better inhibition than 24 h. Besides, free ICG and ICG-MPEG-PCL had same ICG concentration as 5-Fu-ICG-MPEG-PCL, and they exhibited no obvious cytotoxicity without NIR laser.

3.3. The cellular uptake efficiency of 5-Fu-ICG-MPEG-PCL

The results of the cellular uptake efficiencies of 5-Fu-ICG-MPEG-PCL are shown in Fig. 4. For both A431 and A375 cells, the column of ICG was almost black after 1 h of incubation. The red fluorescence of 5-Fu-ICG-MPEG-PCL circled around DAPI stained the cell nucleus after 2 h of incubation, demonstrating that the 5-Fu-ICG-MPEG-PCL was internalized into the cytoplasm of the cells. Also, the fluorescence intensity increased from 1 h to 4 h, suggesting that the cellular uptake efficiencies of the 5-Fu-ICG-MPEG-PCL were time-dependent.

3.4. In vitro photothermal effect of 5-Fu-ICG-MPEG-PCL

We tried to investigate whether the NIR laser could induce the photothermal effect of 5-Fu-ICG-MPEG-PCL to inhibit tumor cell growth. Therefore, we used calcein acetoxymethyl ester (calcein-AM) and propidium iodide (PI) to stain the cells as the live cells (green) and dead cells (red). In Fig. 5, the group of control, control + laser, MPEG-PCL, 5-Fu, 5-Fu-MPEG-PCL, ICG, ICG-MPEG-PCL, and 5-Fu-ICG-MPEG-PCL exhibited green fluorescence of calcein-AM, suggesting that these interventions were safe to cells. Moreover, the cells, treated with ICG + laser, ICG-MPEG-PCL + laser and 5-Fu-ICG-MPEG-PCL + laser, showed red fluorescence of PI, implied that the cells were destroyed due to heat conduction under NIR laser. The MTT assay exhibited the same results. The inhibitory effect on A431 and A375 cells by photothermal effect originated from ICG under an NIR laser is equal, indicating that photothermal therapy has great potentials on treatment of skin cancer.

3.5. Preparation and characterization of microneedle

We successfully prepared 5-Fu-ICG-MPEG-PCL loaded microneedle (5-Fu-ICG-MPEG-PCL@HA MN) with 232.21 ± 53.94 μg of 5-Fu and 27.23 ± 6.33 μg of ICG per patch via a PDMS microneedle master structure [31]. The microneedle with 1 cm × 1 cm was green and had 400 (20 × 20) tips. The tips were lined up in order with a height of 600 μm (Fig. 6A and B). Then we investigated the skin insertion ability of 5-Fu-ICG-MPEG-PCL@HA MN by trypan blue staining method. Consistent blue microchannels of 5-Fu-ICG-MPEG-PCL@HA MN were observed after the insertion of microneedles (Fig. 6C), indicating that the microneedle could penetrate into the skin. Similarly, the histological evaluation (Fig. 6D) exhibited that the 5-Fu-ICG-MPEG-PCL@HA MN could penetrate the cuticle of the skin and deliver the drug transdermal.

3.6. In vitro near-infrared thermal imaging and heating transfer efficacy

Firstly, we studied the *in vitro* photothermal effect of HA MN, 5-Fu-MPEG-PCL@HA MN, ICG-MPEG-PCL@HA MN, and 5-Fu-ICG-MPEG-PCL@HA MN. The results (Fig. 7A) demonstrated that the ICG-MPEG-PCL@HA MN and 5-Fu-ICG-MPEG-PCL@HA MN groups, containing ICG, could quickly reach to 60 °C within 5 min under 1.5 W/cm^2 808 nm NIR laser, implying that these microneedles had good photothermal effect. The temperatures of HA MN and 5-Fu-MPEG-PCL@HA MN groups did not change too much. Besides, we also investigated the heating transfer efficacy of the above-mentioned groups, as the heating transfer efficacy affected the therapeutic effects. In Fig. 8A, the temperatures of HA MN, 5-Fu-MPEG-PCL@HA MN did not change significantly. However, when the pork tissue was treated with ICG-MPEG-PCL@HA MN and 5-Fu-ICG-MPEG-PCL@HA MN, the heat could be transmitted to the center of the pork tissue and rise up to 65 °C within 5 min, and the heat reached to 1.5 cm depth, indicating that the heat could be transferred to the center of the tumor. The heating curves of the *in vitro* photothermal effect (Fig. 7B) and heating transfer efficacy (Fig. 8B) revealed the same trend.

3.7. In vivo near-infrared thermal imaging

Furthermore, we studied the *in vivo* NIR thermal imaging in A431 tumor-bearing balb/cA-nu mice and A375 tumor-bearing balb/cA-nu mice. In Fig. 9A, the control, HA MN, 5-Fu-MPEG-PCL, and 5-Fu-MPEG-PCL@HA MN groups could not increase the temperature of the tumor sites, and the temperature of the tumor sites rose to 50 °C when the tumor was treated with the ICG. Additionally, the temperature of the tumor sites, treated with ICG-MPEG-PCL@HA MN and 5-Fu-ICG-MPEG-PCL@HA MN, was higher than ICG-MPEG-PCL and 5-Fu-ICG-MPEG-PCL groups, because the ICG-MPEG-PCL and 5-Fu-ICG-MPEG-PCL were injected intratumorally, which was not distributed evenly in the tumor tissues, and reduced the heating efficiency at the tumor sites, further proving that microneedles were better drug carriers for transdermal drug delivery. Meanwhile, the heating curves also revealed that the temperature of the tumor tissues could rise up to 50 °C with ΔT of 21 °C within 5 min when the mice were treated with ICG-MPEG-PCL@HA MN and 5-Fu-ICG-MPEG-PCL@HA MN transdermal and under NIR irradiation. The *in vivo* near-infrared thermal imaging of A375 tumor-bearing balb/cA-nu mice (Fig. S2) was almost similar to those of A431 tumor-bearing balb/cA-nu mice.

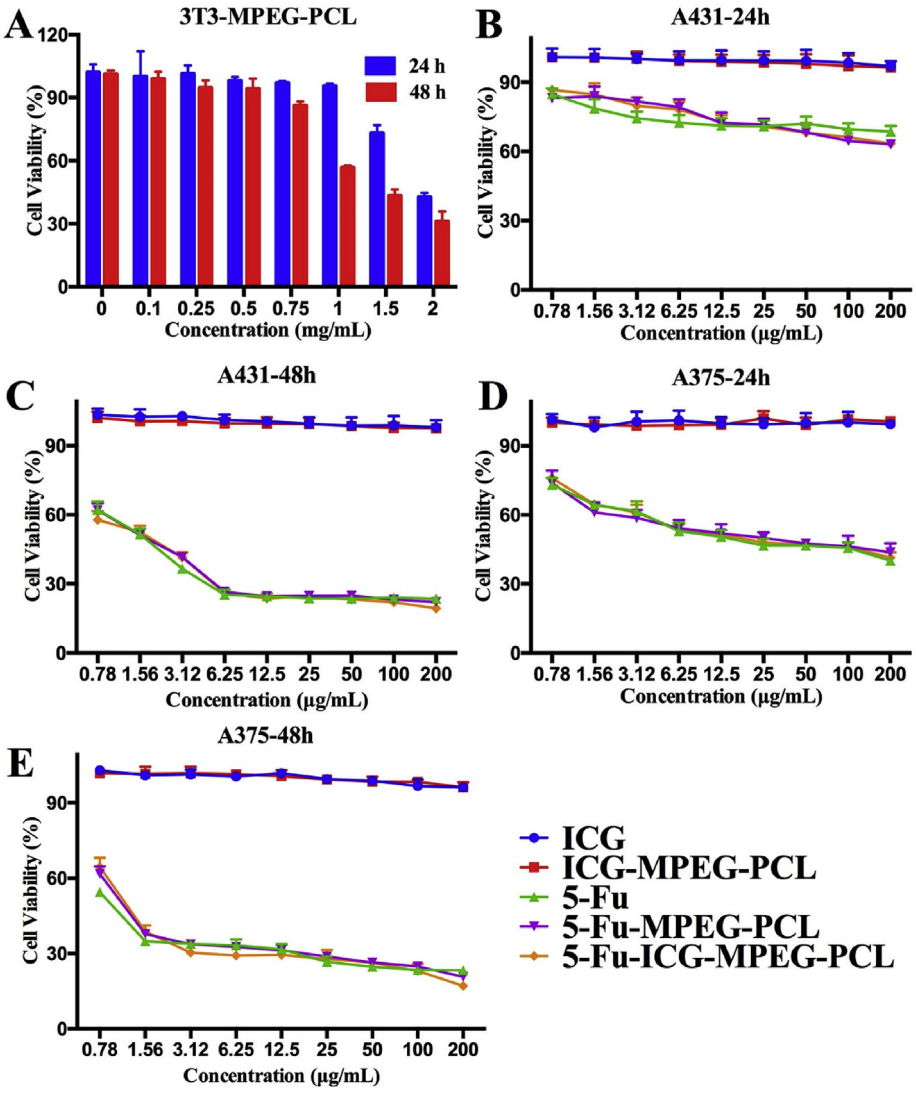

Fig. 3. *In vitro* cytotoxicity study of (A) 3T3 cells treated with MPEG-PCL after 24 h and 48 h of incubation, A431 cells treated with different nanoparticle after (B) 24 h and (C) 48 h of incubation and A375 cells treated with different nanoparticle after (D) 24 h and (E) 48 h of incubation.

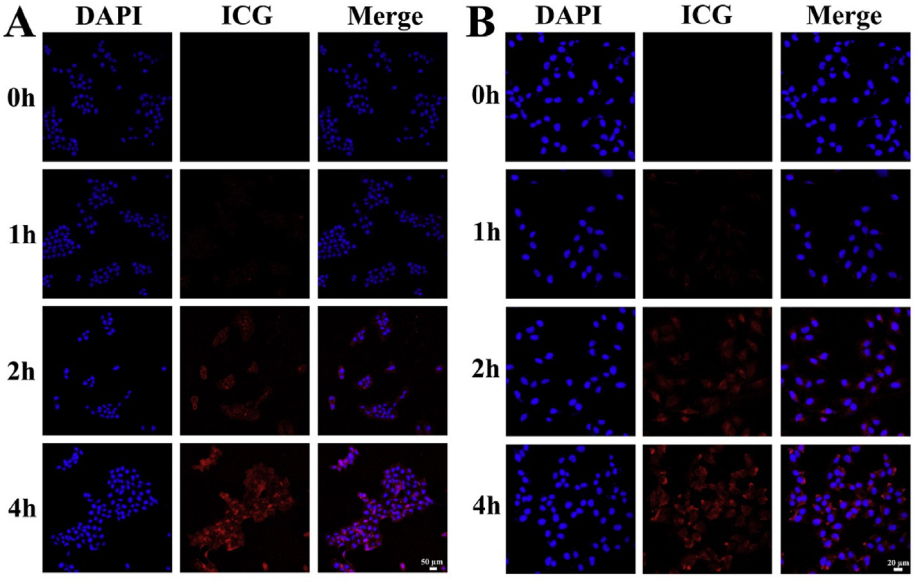

Fig. 4. The cellular uptake ability of (A) A431 cells (scale bar: 50 μm) and (B) A375 cells (scale bar: 20 μm).

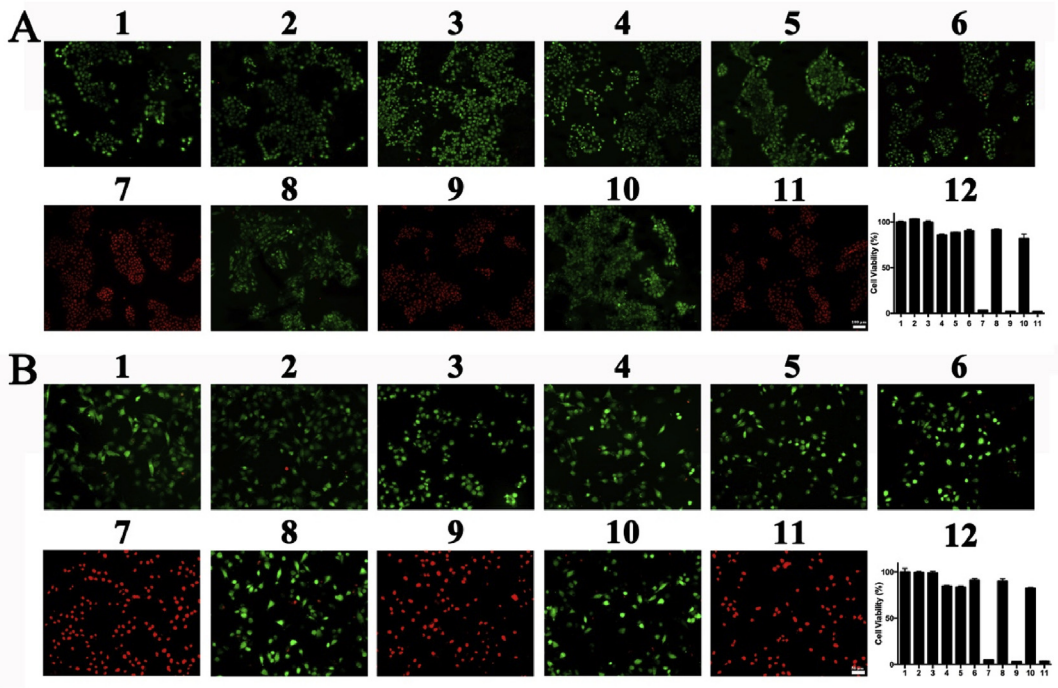

Fig. 5. The image of (A) A431 cells (scale bar: 100 μm) and (B) A375 cells (scale bar: 50 μm) stained by calcein AM/PI with different treatments. (1. Control, 2.Control + Laser, 3.MPEG-PCL, 4.5-Fu, 5.5-Fu-MPEG-PCL, 6. ICG, 7.ICG + Laser, 8.ICG-MPEG-PCL, 9.ICG-MPEG-PCL + Laser, 10. 5-Fu-ICG-MPEG-PCL, 11. 5-Fu-ICG-MPEG-PCL + Laser, 12.the cell viability after different treatments.)

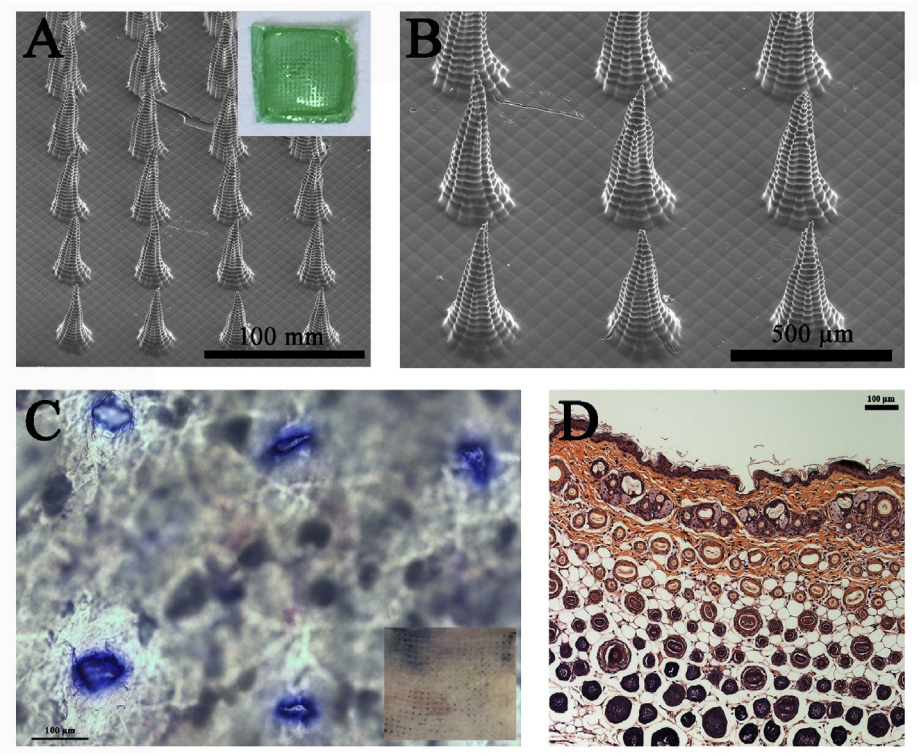

Fig. 6. (A, B) SEM images of the 5-Fu-ICG-MPEG-PCL@HA MN (The photograph of 5-Fu-ICG-MPEG-PCL@HA MN is inserted). (C) optical micrograph (scale bar:100 μm, the photograph of skin was inserted) and (D) histological sections (scale bar, 100 μm) of the mice skin stained with trypan blue after 5-Fu-ICG-MPEG-PCL@HA MN application.

3.8. In vivo antitumor efficacy

Finally, we studied the *in vivo* antitumor ability of 5-Fu-ICG-MPEG-PCL@HA MN in A431 tumor-bearing balb/cA-nu mice and A375 tumor-bearing balb/cA-nu mice. In Fig. 10A, the tumor growth curves of the control and HA MN groups displayed rapid growth. In 5-Fu-MPEG-PCL, ICG-MPEG-PCL + laser, and 5-Fu-MPEG-PCL@HA MN groups, the tumor volumes were reduced, but the therapeutic effect was not as obvious as a single-chemotherapy or photothermal therapy. The intratumor administration of 5-Fu-ICG-MPEG-PCL under NIR irradiation exhibited better antitumor ability than the above 3 groups because of the synergistic chemotherapy and photothermal therapy. The 5-Fu-ICG-MPEG-PCL@HA MN + laser group exhibited the greatest tumor inhibition, the mice were all cured without recurrence, which further

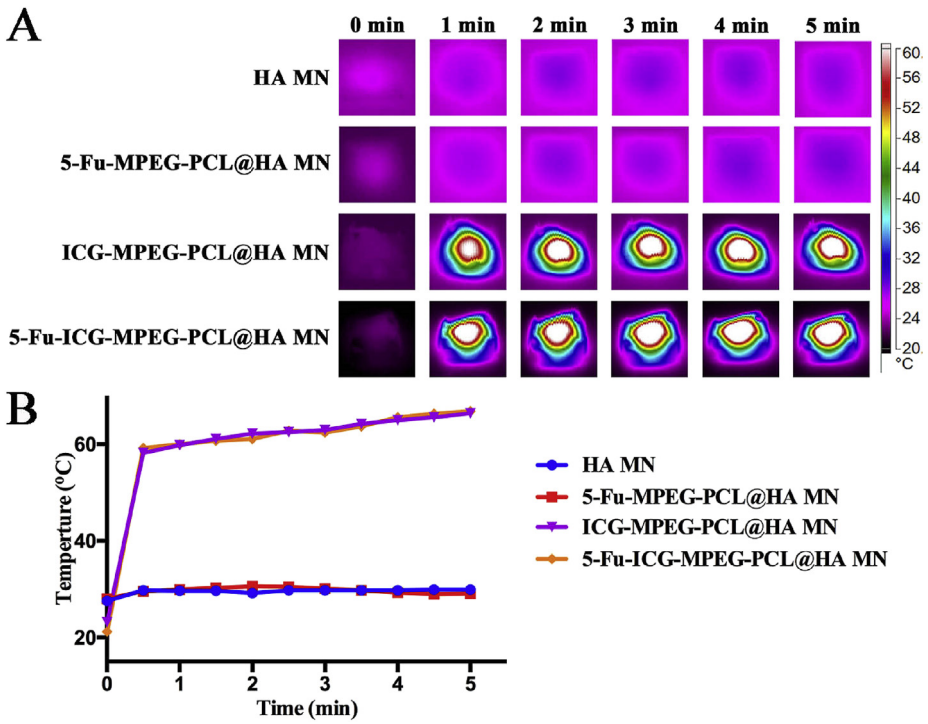

Fig. 7. (A) The near-infrared thermal imaging of different microneedles within 5 min (1.5 W/cm^2, 808 nm laser). (B) The heating curves of the microneedles.

demonstrated that the combination therapy could improve the anti-tumor ability, and the microneedle was a remarkable drug carrier. Besides, the mice treated with ICG-MPEG-PCL@HA MN inhibited the tumor growth in early time, but the tumor could recur, implying that the microneedle without chemical drug could not inhibit the recurrence of the tumor. The body-weights of all groups were not changed significantly (Fig. 10B), indicating that the treatment was safe. The photographs and weights of the subcutaneous tumors in all groups are displayed in Fig. 10C and D. Meanwhile, the H&E staining images of major organ tissues (Fig. S3) presented no lesions or inflammation in all groups, suggesting that the microneedle transdermal administration was a safe method. Additionally, A375 tumor-bearing balb/cA-nu mice were used for studying the anti-tumor ability of 5-Fu-ICG-MPEG-PCL@HA MN, the results (Fig. 11) showed that the 5-Fu-ICG-MPEG-PCL@HA MN + laser group could also cure the tumor without recurrence. These results have implied that the as-made microneedle system has a wide application prospect for skin cancer treatment.

3.9. The histopathological and proliferation study of the tumor cells

We also studied the histopathological and immune histochemical of all groups (Fig. S4). After H&E staining the tumors, the group, treated with ICG-MPEG-PCL@HA MN + laser, exhibited seriously damaged tumor cells. Additionally, we also investigated the apoptosis and

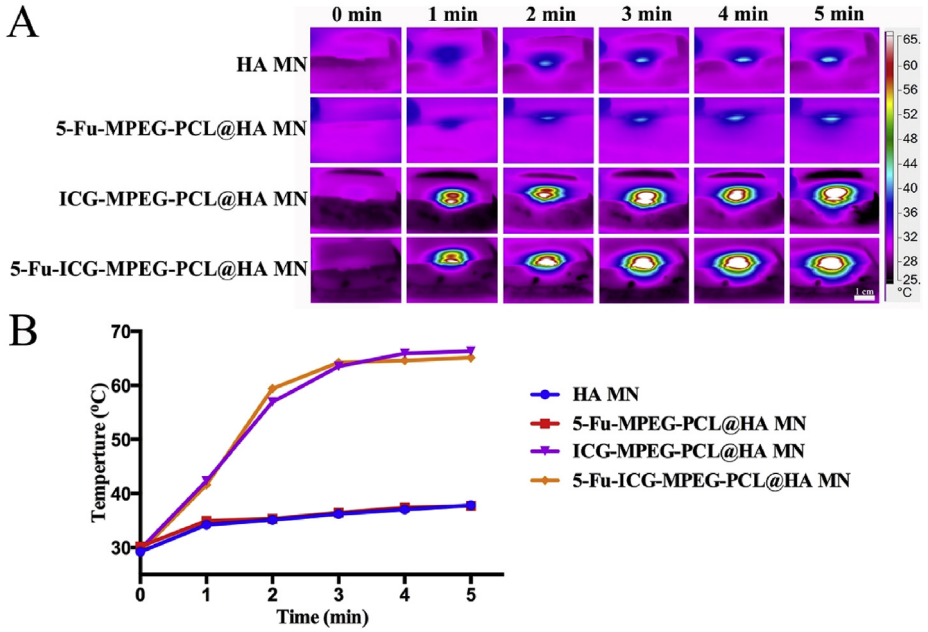

Fig. 8. (A) The heat-transfer efficacy in pork tissue within 5 min (1.5 W/cm^2, 808 nm laser, scale bar: 1 cm). (B) The center temperature curves of the pork tissue.

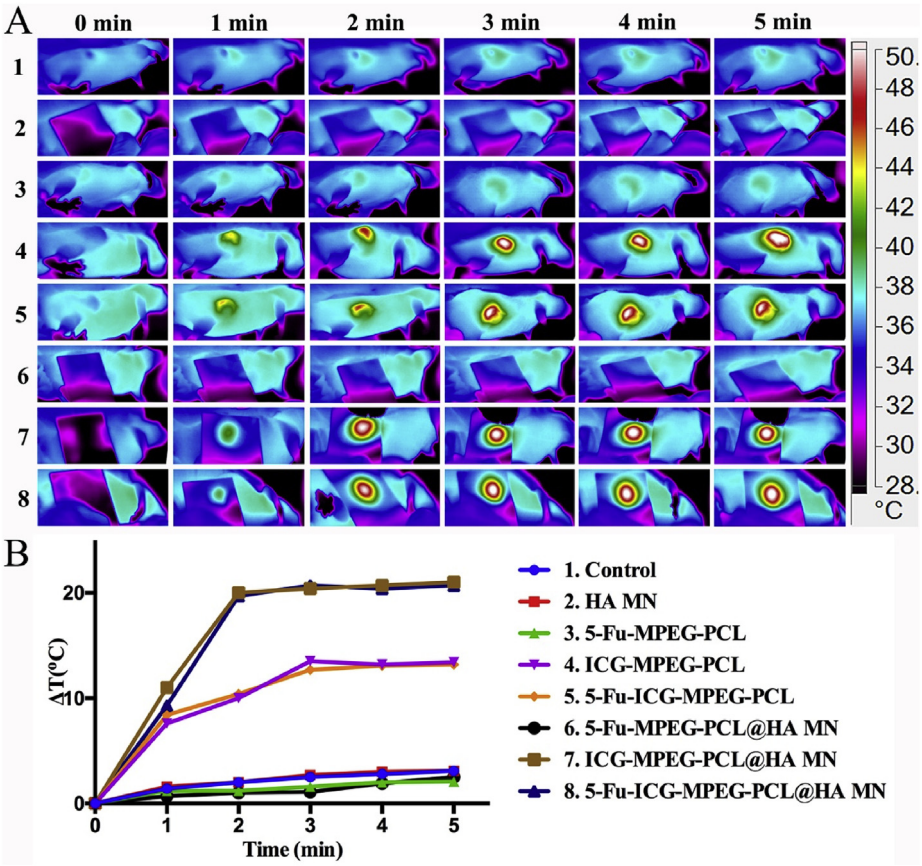

Fig. 9. (A) The near-infrared photothermal effect on A431 tumor-bearing mice within 5 min (1.5 W/cm^2, 808 nm laser). (B) The temperature change curves in the tumor sites.

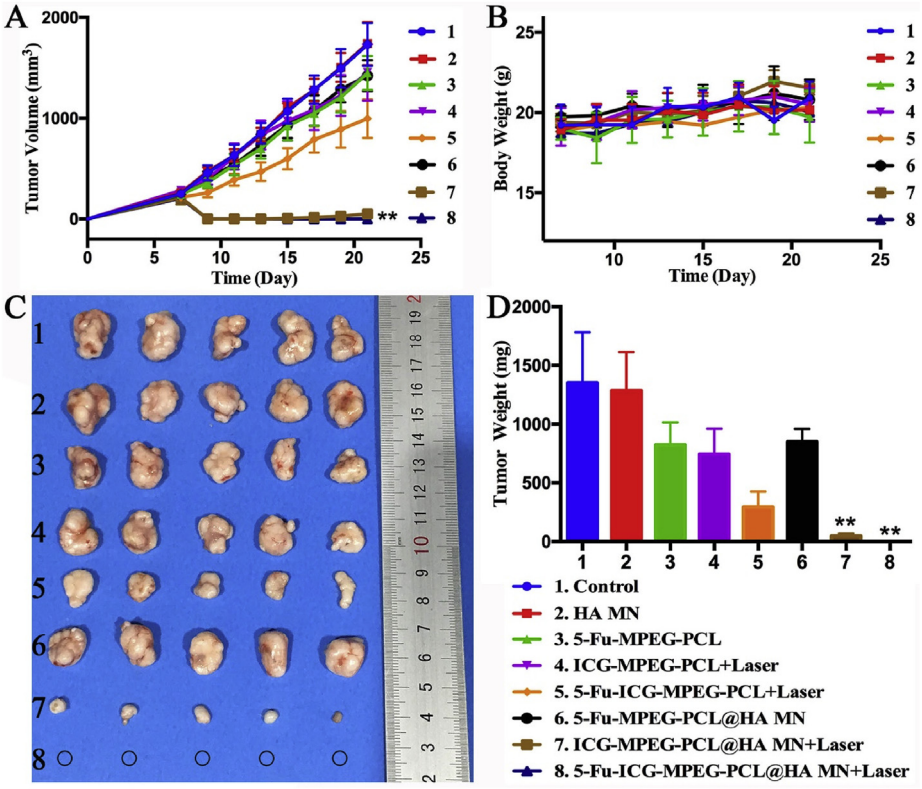

Fig. 10. (A) The growth curves and (B) body weights of A431 tumor-bearing mice in each group. (C) The photograph and (F) weights of subcutaneous tumors in each group (the black circle represents the location of cured tumors). The data are represented as the mean ± standard deviation (n = 5). "**" indicated P < 0.01.

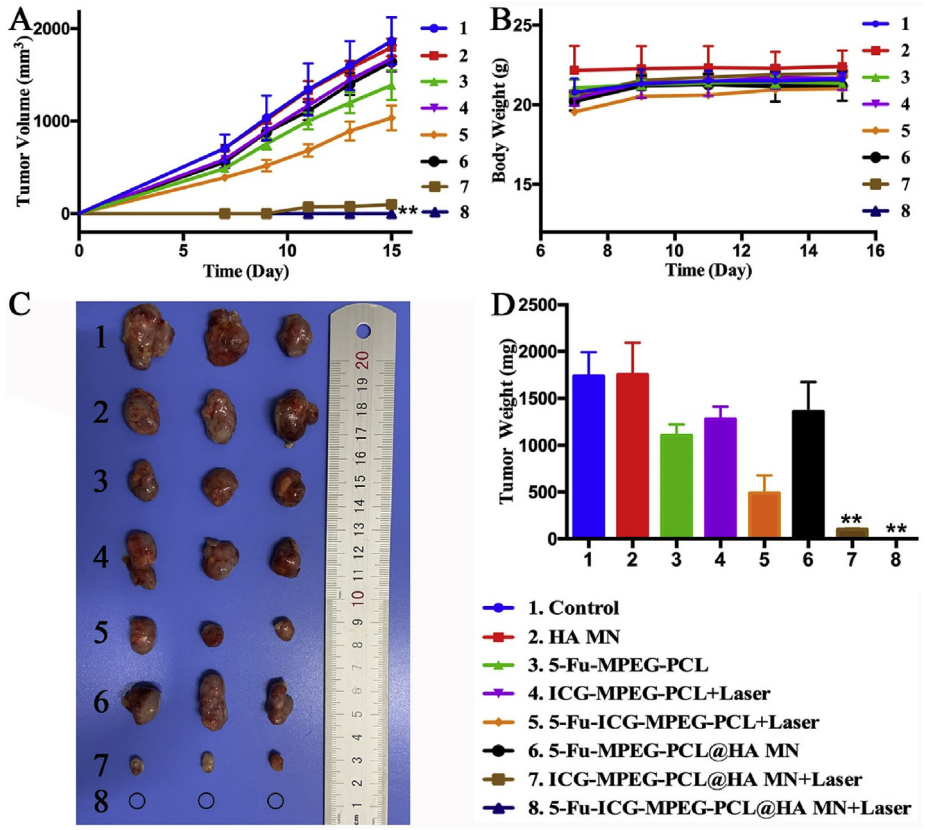

Fig. 11. (A) The growth curves and (B) body weights of A375 tumor-bearing mice in each group. (C) The photographs and (F) weight of subcutaneous tumors in each group (the black circle represents the location of cured tumors). Data are represented as the mean ± standard deviation (n = 5). "**" indicates P < 0.01.

proliferation of the tumor cells via tunel staining and Ki67 staining. The highest level of the cell apoptosis was noticed in ICG-MPEG-PCL@HA MN + laser group, and the cell proliferation was consistent with apoptosis. These results demonstrated that the photothermal therapy is a better method for skin cancer treatment.

4. Conclusion

In conclusion, the 5-Fu-ICG-MPEG-PCL with uniform size produced good photothermal effect and effectively inhibited the proliferation of A431 and A375 cells. Then, the 5-Fu-ICG-MPEG-PCL was integrated with HA MN to obtain NIR-responsive 5-Fu-ICG-MPEG-PCL@HA MN. The 5-Fu-ICG-MPEG-PCL@HA MN exhibited good skin insertion ability and heat-transfer efficacy. Meanwhile, it also possessed good photothermal effect, which not only thermally ablated tumor, but also controlled the release behavior of 5-Fu in the nanoparticles to achieve synergistic chemotherapy and photothermal therapy of skin cancer. Furthermore, both for the A431 tumor-bearing balb/cA-nu mice and A375 tumor-bearing balb/cA-nu mice, the 5-Fu-ICG-MPEG-PCL@HA MN exhibited promising anti-tumor ability and could cure the tumor without any recurrence. Therefore, this NIR-responsive 5-Fu-ICG-MPEG-PCL@HA MN could inhibit the tumor growth of human epidermoid cancer and melanoma, which could be applied in skin cancer therapy.

Declaration of competing interest

The authors declare no competing financial interest.

Acknowledgements

This work was financially supported by the National Natural Science Foundation of China (No. 31525009, 31930067, 31771096), West China Precision Medicine Industrial Technology Institutes (2018-CY02-00058-GX), National Key Research and Development Program of China (No. 2017YFC1103502), and 1·3·5 project for disciplines of excellence, West China Hospital, Sichuan University (ZYGD18002). National Clinical Research Center for Geriatrics, West China Hospital, Sichuan University (Z2018B06). Post-Doctor Research Project, West China Hospital, Sichuan University (2018HXBH043), China Postdoctoral Science Foundation (2019M653410), The Postdoctoral Innovation Talents Support Program (BX20180207).

We thank Dr. Hui Wang from the Analytical & Testing center, Sichuan University, P. R. China for the SEM observation and analysis of the data.

Appendix A. Supplementary data

Supplementary data to this article can be found online at https://doi.org/10.1016/j.bioactmat.2020.04.002.

References

[1] S. Aractingi, J. Kanitakis, S. Euvrard, C.L. Danff, I. Peguillet, K. Khosrotehrani, O. Lantz, E.D. Carosella, Skin carcinoma arising from donor cells in a kidney transplant recipient, Canc. Res. 65 (5) (2005) 1755–1760.
[2] R.L. Siegel, K.D. Miller, A. Jemal, Cancer statistics, Ca - Cancer J. Clin. 70 (1) (2020) 7–30 2020.
[3] A. Esteva, B. Kuprel, R.A. Novoa, J. Ko, S.M. Swetter, H.M. Blau, S. Thrun, Dermatologist-level classification of skin cancer with deep neural networks, Nature 542 (7639) (2017) 115–118.
[4] K.D. Miller, L. Nogueira, A.B. Mariotto, J.H. Rowland, K.R. Yabroff, C.M. Alfano, A. Jemal, J.L. Kramer, R.L. Siegel, Cancer treatment and survivorship statistics, Ca - Cancer J. Clin. 69 (5) (2019) 363–385 2019.
[5] J. Chen, T. Fan, Z. Xie, Q. Zeng, P. Xue, T. Zheng, Y. Chen, X. Luo, H. Zhang, Advances in nanomaterials for photodynamic therapy applications: status and challenges, Biomaterials 237 (2020) 119827.

[6] Z.H. Yu, Y.C. Guo, H. Dai, B.F. Zeng, X. Zheng, C.X. Yi, N. Jiang, Y. Liu, X. Huang, On-demand drug release and re-absorption from pirarubicin loaded Fe3O4@ZnO core-shell nanoparticles for targeting infusion chemotherapy for urethral carcinoma, Mater Express 9 (2019) 467–474.
[7] R.S. Riley, C.H. June, L. Robert, M.J. Mitchell, Delivery technologies for cancer immunotherapy, Nat. Rev. Drug Discov. 8 (2019) 175–196.
[8] Y. Hao, W. Li, X. Zhou, F. Yang, Z. Qian, Microneedles-based transdermal drug delivery systems: a review, J. Biomed. Nanotechnol. 13 (12) (2017) 1581–1597.
[9] X.L. Zhou, Y. Hao, L.P. Yuan, S. Pradhan, W. Li, Nano-formulations for transdermal drug delivery: a review, Chin. Chem. Lett. 29 (12) (2018) 1713–1724.
[10] P. Dardano, M. Battisti, I. Rea, L. Serpico, M. Terracciano, A. Cammarano, L. Nicolais, L.D. Stefano, Polymeric microneedle arrays: versatile tools for an innovative approach to drug administration, Adv. Ther. 2 (2019) 1900036.
[11] C. Bellefroid, A. Lechanteur, B. Evrard, D. Mottet, F. Debacq-Chainiaux, G. Piel, In vitro skin penetration enhancement techniques: a combined approach of ethosomes and microneedles, Int. J. Pharm. 572 (2019) 118793.
[12] G.S. Liu, Y. Kong, Y. Wang, Y. Luo, X. Fan, X. Xie, B.R. Yang, M.X. Wu, Microneedles for transdermal diagnostics: recent advances and new horizons, Biomaterials 232 (2020) 119740.
[13] J. Yang, X. Liu, Y. Fu, Y. Song, Recent advances of microneedles for biomedical applications: drug delivery and beyond, Acta Pharm. Sin. B 9 (3) (2019) 469–483.
[14] P. Singh, A. Carrier, Y. Chen, S. Lin, J. Wang, S. Cui, X. Zhang, Polymeric microneedles for controlled transdermal drug delivery, J. Contr. Release 315 (2019) 97–113.
[15] S. Babity, M. Roohnikan, D. Brambilla, Advances in the design of transdermal microneedles for diagnostic and monitoring applications, Small 14 (49) (2018) 1803186.
[16] Y. Ye, C. Wang, X. Zhang, Q. Hu, Y. Zhang, Q. Liu, D. Wen, J. Milligan, A. Bellotti, L. Huang, G. Dotti, Z. Gu, A melanin-mediated cancer immunotherapy patch, Sci immunol 2 (17) (2017) 5692.
[17] Y. Ye, J. Yu, D. Wen, A.R. Kahkoska, Z. Gu, Polymeric microneedles for transdermal protein delivery, Adv. Drug Deliv. Rev. 127 (2018) 106–118.
[18] M.J. Uddin, N. Scoutaris, S.N. Economidou, C. Giraud, B.Z. Chowdhry, R.F. Donnelly, D. Douroumis, 3D printed microneedles for anticancer therapy of skin tumours, Mater. Sci. Eng. C 107 (2020) 110248.
[19] Y. Hao, M. Dong, T. Zhang, J. Peng, Y. Jia, Y. Cao, Z. Qian, Novel approach of using near-infrared responsive PEGylated gold nanorod coated poly(l-lactide) microneedles to enhance the antitumor efficiency of docetaxel-loaded MPEG-PDLLA micelles for treating an A431 tumor, ACS Appl. Mater. Interfaces 9 (18) (2017) 15317–15327.
[20] Y. Hao, Y. Chen, M. Lei, T. Zhang, Y. Cao, J. Peng, L. Chen, Z. Qian, Near-infrared responsive PEGylated gold nanorod and doxorubicin loaded dissolvable hyaluronic acid microneedles for human epidermoid cancer therapy, Adv. Ther. 1 (2) (2018) 1800008.
[21] R. Petrilli, J.O. Eloy, F.P. Saggioro, D.L. Chesca, M.C. de Souza, M.V.S. Dias, L.L.P. daSilva, R.J. Lee, R.F.V. Lopez, Skin cancer treatment effectiveness is improved by iontophoresis of EGFR-targeted liposomes containing 5-FU compared with subcutaneous injection, J. Contr. Release 283 (2018) 151–162.
[22] A.R. Rosenberg, M. Tabacchi, K.H. Ngo, M. Wallendorf, I.S. Rosman, L.A. Cornelius, S. Demehri, Skin cancer precursor immunotherapy for squamous cell carcinoma prevention, JCI Insight 4 (6) (2019).
[23] C.W. Ji, A. Yuan, L. Xu, F.F. Zhang, S.W. Zhang, X.Z. Zhao, G.X. Liu, W. Chen, H.Q. Guo, Activatable photodynamic therapy for prostate cancer by NIR dye/photosensitizer loaded albumin nanoparticles, J. Biomed. Nanotechnol. 15 (2019) 311–318.
[24] J.S. Treger, M.F. Priest, R. Iezzi, F. Bezanilla, Real-time imaging of electrical signals with an infrared FDA-approved dye, Biophys. J. 107 (6) (2014) 09-12.
[25] J. Zhu, X. Tang, Y. Jia, C.T. Ho, Q. Huang, Applications and delivery mechanisms of hyaluronic acid used for topical/transdermal delivery-A review, Int. J. Pharm. 578 (2020) 119127.
[26] J. Zhu, L. Dong, H. Du, J. Mao, Y. Xie, H. Wang, J. Lan, Y. Lou, Y. Fu, J. Wen, B. Jiang, Y. Li, J. Zhu, J. Tao, 5-Aminolevulinic acid-loaded hyaluronic acid dissolving microneedles for effective photodynamic therapy of superficial tumors with enhanced long-term stability, Adv Healthc Mater 8 (22) (2019) 1900896.
[27] Y. Hao, Y. Huang, Y. He, J. Peng, L. Chen, X. Hu, Z. Qian, The evaluation of cellular uptake efficiency and tumor-targeting ability of MPEG–PDLLA micelles: effect of particle size, RSC Adv. 6 (17) (2016) 13698–13709.
[28] D. Hu, L. Chen, Y. Qu, J. Peng, B. Chu, K. Shi, Y. Hao, L. Zhong, M. Wang, Z. Qian, Oxygen-generating Hybrid Polymeric Nanoparticles with Encapsulated Doxorubicin and Chlorin e6 for Trimodal Imaging-Guided Combined Chemo-Photodynamic Therapy, Theranostics 8 (6) (2018) 1558–1574.
[29] Y. Hao, J. Peng, Y. Zhang, L. Chen, F. Luo, C. Wang, Z. Qian, Tumor neovasculature-targeted APRPG-PEG-PDLLA/MPEG-PDLLA mixed micelle loading combretastatin A-4 for breast cancer therapy, ACS Biomater. Sci. Eng. 4 (6) (2017) 1986–1999.
[30] S.Q. Yang, L.Z. Zhou, Y. Su, R. Zhang, C.M. Dong, One-pot photoreduction to prepare NIR-absorbing plasmonic gold nanoparticles tethered by amphiphilic polypeptide copolymer for synergistic photothermal-chemotherapy, Chin. Chem. Lett. 30 (1) (2019) 187–191.
[31] Y. Hao, H. Li, Y. Cao, Y. Chen, M. Lei, T. Zhang, Y. Xiao, B.Y. Chu, Z. Qian, Uricase and horseradish peroxidase hybrid CaHPO4 nanoflower integrated with transcutaneous patches for treatment of hyperuricemia, J. Biomed. Nanotechnol. 15 (5) (2019) 951–965.
[32] Q. Jin, H.J. Chen, X. Li, X. Huang, Q. Wu, G. He, T. Hang, C. Yang, Z. Jiang, E. Li, A. Zhang, Z. Lin, F. Liu, X. Xie, Reduced graphene oxide nanohybrid-assembled microneedles as mini-invasive electrodes for real-time transdermal biosensing, Small 15 (6) (2019) 1804298.
[33] H. Du, P. Liu, J. Zhu, J. Lan, Y. Li, L. Zhang, J. Zhu, J. Tao, Hyaluronic acid-based dissolving microneedle patch loaded with methotrexate for improved treatment of psoriasis, ACS Appl. Mater. Interfaces 11 (46) (2019) 43588–43598.